Comparative study of the free-surface boundary condition in two-dimensional finite-difference elastic wave field simulation

2011 J. Geophys. Eng. 8 275

(http://iopscience.iop.org/1742-2140/8/2/012)

IOP Publishing Journal of Geophysics and Engineering
J. Geophys. Eng. **8** (2011) 275–286 doi:10.1088/1742-2132/8/2/012

Comparative study of the free-surface boundary condition in two-dimensional finite-difference elastic wave field simulation

Haiqiang Lan and Zhongjie Zhang

State Key Laboratory of Lithospheric Evolution, Institute of Geology and Geophysics, Chinese Academy of Sciences, Beijing 100029, People's Republic of China

E-mail: lanhq@mail.iggcas.ac.cn

Received 16 December 2010
Accepted for publication 2 March 2011
Published 28 March 2011
Online at stacks.iop.org/JGE/8/275

Abstract
The finite-difference (FD) method is a powerful tool in seismic wave field modelling for understanding seismic wave propagation in the Earth's interior and interpreting the real seismic data. The accuracy of FD modelling partly depends on the implementation of the free-surface (i.e. traction-free) condition. In the past 40 years, at least six kinds of free-surface boundary condition approximate schemes (such as one-sided, centred finite-difference, composed, new composed, implicit and boundary-modified approximations) have been developed in FD second-order elastodynamic simulation. Herein we simulate seismic wave fields in homogeneous and lateral heterogeneous models using these free-surface boundary condition approximate schemes and evaluate their stability and applicability by comparing with corresponding analytical solutions, and then quantitatively evaluate the accuracies of different approximate schemes from the misfit of the amplitude and phase between the numerical and analytical results. Our results confirm that the composed scheme becomes unstable for the V_s/V_p ratio less than 0.57, and suggest that (1) the one-sided scheme is only accurate to first order and therefore introduces serious errors for the shorter wavelengths, other schemes are all of second-order precision; (2) the new composed, implicit and boundary-modified schemes are stable even when the V_s/V_p ratio is less than 0.2; (3) the implicit and boundary-modified schemes are able to deal with laterally varying (heterogeneous) free surface; (4) in the corresponding stability range, the one-sided scheme shows remarkable errors in both phase and amplitude compared to analytical solution (which means larger errors in travel-time and reflection strength), the other five approximate schemes show better performance in travel-time (phase) than strength (amplitude).

Keywords: free-surface boundary condition, finite-difference modelling, stability, accuracy

1. Introduction

The real surface of the Earth is an impedance-mutated interface of a half-space in contact with vacuum, known as free surface. This topography leads to tremendous influences upon seismic exploration of hydrocarbon and non-hydrocarbon resources or deep structure of the Earth's interior, such as decreasing signal to noise ratio of seismic data from irregular topography. In order to interpret real seismic data and understand seismic wave propagation in the Earth's interior, the free-surface boundary condition must be satisfied at the top boundary of the model. In principle, it is very simple to assume the boundary condition as the surface with zero vertical stress (stress-free surface), but it is still a challenge in numerical simulation of seismic wave propagation.

Parallel to the development of absorbing boundary conditions in 2 and 3D media (Clayton and Enquist 1977,

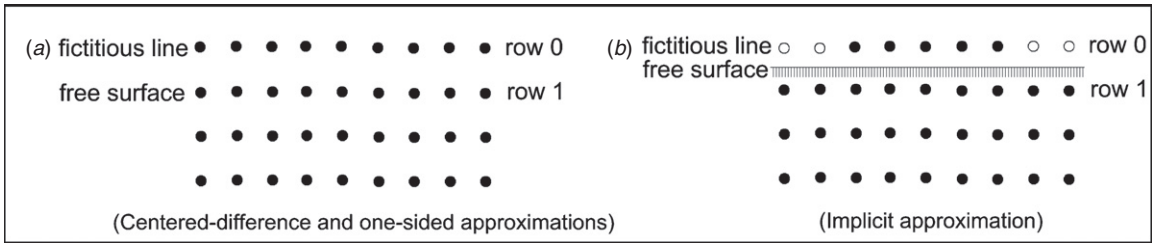

Figure 1. The grid imposed on the half plane as used in the centred difference, one-sided approximations (*a*) and implicit approximation (*b*).

Engquist and Majda 1977, Reynolds 1978, Liao *et al* 1984, Cerjan *et al* 1985, Higdon 1991, Zhang *et al* 1993, 1999, Berenger 1994, Cao and Greenhalgh 1998, Yang *et al* 2002, 2003, Komatitsch and Tromp 2003, Wu and Liang 2005, Tian *et al* 2008, Chen and Bording 2010), numerous methods to deal with the free-surface boundary condition have been proposed in the past four decades since the development of finite-difference approximations of the elastodynamic equations in second-order formulation (Alterman and Karal 1968, Alterman and Rotenberg 1969). These schemes can be divided into two kinds: (1) adding a fictitious layer above the free surface (figure 1), which includes a centred finite-difference approximation (Alterman and Karal 1968), a one-sided approximation (Alterman and Rotenberg 1969) and an implicit boundary update technique (Vidale and Clayton 1986).

In all these three approximations the derivatives with respect to x are replaced by central differences. These approximations differ in the way in which the normal derivatives are represented. The first two approximations are explicit, for approximation 1 (centred), centred differences are used, while for approximation 2 (one sided), one-sided differences are used to express the first-order derivatives with respect to z along the free surface. The third approximation uses an implicit formulation which centres both the normal and tangential derivatives at the free surface, halfway between row 0 and row 1. The scheme is similar in concept to the Crank–Nicholson method for the diffusion equation (Crank and Nicolson 1996). More details on these three approximations can be found in appendix A.

(2) Substitution of the derivatives normal to the free surface without any fictitious layer above the free surface (figure 2). This also includes three schemes: a composed approximation (Ilan *et al* 1975), a remedy scheme (new composed approximation) (Ilan and Loewenthal 1976, Ilan 1978) and also a boundary-modified difference approximation (Nilsson *et al* 2007, Lan and Zhang 2011).

The composed approximation is based on an approach which was developed by Ilan *et al* (1975). According to this approach the z derivatives on the free surface are first replaced by x and t derivatives, by using the equations of motion. Then centred differences are applied. Due to the substitution of the derivatives normal to the free surface no fictitious line is required. More details on this approximation can be found in appendix B.

The composed approximation could not handle the case where the ratio of the shear (S) to compressional (P) wave velocities (V_s/V_p) is less than 0.57 (Ilan *et al* 1975). Ilan and Loewenthal (1976) and Ilan (1978) proposed a revised method (new composed approximation) (refer to appendix C for more details).

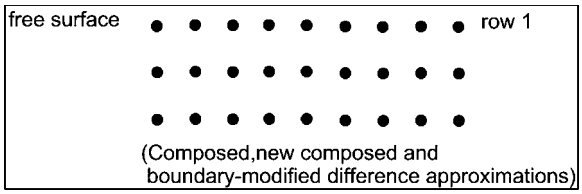

Figure 2. The grid imposed on the half plane as used in the composed, new composed and boundary-modified difference approximations.

The boundary-modified difference approximation is a stable and explicit discretization of the free-surface boundary conditions presented by Nilsson *et al* (2007). In summary, they introduced a discretization that uses boundary-modified difference operators for the mixed derivatives in the governing equations and showed that the method is second-order accurate for problems with smoothly varying material properties and stable under standard Courant–Friedrichs–Lewy constraints, for arbitrarily varying material properties (refer to appendix D for more details). Lan and Zhang (2011) extended the scheme in modelling the 3D–3C wave field in the anisotropic medium with an irregular free surface.

In this study, we compare the above approximate methods for dealing with the free-surface boundary condition.

2. Wave equation and the free-surface boundary condition

In order to facilitate the treatment of the free-surface boundary condition presented here we consider an elastic half space case, as the free-surface boundary condition of zero-vertical stress components is always valid, and this simplification leads to the classical Lamb's problem (Lamb 1904) and its analytical solution (De Hoop 1960) provides a standard reference to check the accuracy of different approximations of the free-surface boundary condition in the finite difference wave field modelling.

Let the x axis be parallel to the horizontal free surface and the z axis pointing vertically downwards. The free surface is assumed to be along $z = 0$ and the half space is contained in the region with $z \geqslant 0$. Let u and v be the horizontal and vertical displacements in the x and z directions, respectively.

The elastic equations of wave motion in isotropic media are

$$\rho\frac{\partial^2 u}{\partial t^2} = \frac{\partial}{\partial x}\left((\lambda+2\mu)\frac{\partial u}{\partial x}+\lambda\frac{\partial v}{\partial z}\right)+\frac{\partial}{\partial z}\left(\mu\frac{\partial u}{\partial z}+\mu\frac{\partial v}{\partial x}\right), \tag{1}$$

$$\rho\frac{\partial^2 v}{\partial t^2} = \frac{\partial}{\partial x}\left(\mu\frac{\partial v}{\partial x}+\mu\frac{\partial u}{\partial z}\right)+\frac{\partial}{\partial z}\left((\lambda+2\mu)\frac{\partial v}{\partial z}+\lambda\frac{\partial u}{\partial x}\right), \tag{2}$$

where $\lambda(x,\ z)$ and $\mu(x,\ z)$ are elastic parameters; $\rho(x,\ z)$ is density.

The classic free-surface boundary conditions on $z = 0$ for the tangential and normal stress components are

$$\mu\frac{\partial u}{\partial z}+\mu\frac{\partial v}{\partial x} = 0, \tag{3}$$

$$(\lambda+2\mu)\frac{\partial v}{\partial z}+\lambda\frac{\partial u}{\partial x} = 0. \tag{4}$$

A grid is imposed on the xz plane (see figures 1 and 2) in finite difference modelling of elastic wave field. The grid implies the spatial discretizations performed along the x and z axes with equal spacing of $\Delta x, \Delta z$, respectively. A further discretization is assumed in time, $x = i\Delta x$; $z = j\Delta z$;$t = p\Delta t$ with $i,\ j$ and p integers. In order to simplify notation we assume equal spatial increments $\Delta x = \Delta z = h$. The standard finite difference approximations to the elastic wave equation (Kelly *et al* 1976) can be used to determine the solution on the inner points. Along the boundary points of the grid which coincides with the free surface a special treatment, which uses the boundary condition given by equations (3) and (4), is needed. Note that the problem is how to deal with above equations (equations (3) and (4)) as the free-surface boundary condition in the finite difference modelling using equations (1) and (2).

3. Comparison of the stability and accuracy of the different free-surface boundary approximate schemes

To evaluate the performance of the six approximate schemes mentioned above for the free-surface boundary condition, in the following we compare the stability and accuracy of different free-surface boundary approximate schemes with the analytical solution of De Hoop (1960) in a homogeneous half space (which includes three models) and a lateral heterogeneous model, respectively. Ilan *et al* (1975) suggested that the composed approximation method cannot handle the case where the ratio of the shear (S) to compressional (P) wave velocities (V_s/V_p) is less than 0.57. In order to discuss the performance of different free-boundary condition approximate schemes at different V_s/V_p ratios, we design three homogeneous half models with V_s/V_p ratios of 0.725, 0.43 and 0.2, respectively. In the following modelling, we assume a vertical point source:

$$f(t) = \mathrm{e}^{-0.5 f_0^2 (t-t_0)^2}\cos\pi f_0(t-t_0), \tag{5}$$

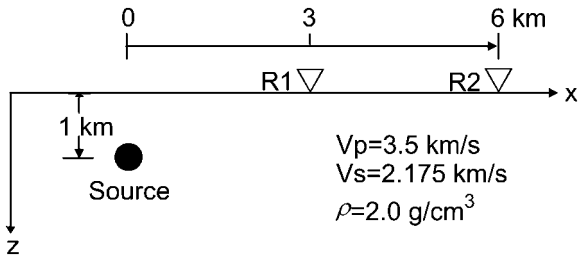

Figure 3. The first model of a homogeneous half-space.

with $t_0 = 0.5$ s for the former two homogeneous models and changed to 2.0 s for the third homogeneous model located at a point 1 km below the free surface. The source–receiver distance ranges from $3\lambda^s_{\mathrm{dom}}$ to $15\lambda^s_{\mathrm{dom}}$ (λ^s_{dom} is the dominant wavelength of the S waves); this range is typical in the study of earthquake ground motion modelling in sedimentary valleys and basins.

3.1. Homogeneous half-space models

3.1.1. Model 1. Figure 3 is a half-space elastic medium with the free surface as a test model. The P-velocity is 3000 m s^{-1}, the S-velocity 2175 m s^{-1}, and the density 2500 kg m^{-3}. Thus, the dominant and minimum wavelengths of the S wave are $\lambda^s_{\mathrm{dom}} = 290$ m and $\lambda^s_{\mathrm{min}} = 145$ m (λ^s_{min} is the minimum wavelength of the S waves), respectively. The high cut-off frequency is 10 Hz, the grid spacing is 10 m and the time step is 1.5 ms. Different free-surface implementations are compared with the analytical solution of De Hoop (1960). We present waveforms with the offsets of 3 and 6 km, respectively (figures 4 and 5). From figures 4 and 5, we can see that all the numerical methods are stable and produce accurate results for this model. The slight differences in sharpness between the analytical solution and the finite-difference trace are due to the grid dispersion in the finite-difference method; the deviations become greater as the propagation distance increases. The surface wave dispersion is more severe than body waves.

3.1.2. Model 2. The elastic parameters for this model are: the P-velocity is 3500 m s^{-1}, the S-velocity 1500 m s^{-1}, and the density 2000 kg m^{-3}. The ratio of the S- to P-wave velocities is about 0.43. The high cut-off frequency is 10 Hz, the grid spacing is 10 m and the time step is 1.5 ms. Figures 6 and 7 show the horizontal and vertical components of the particle displacement, respectively, with the offset of 4 km. The new composed scheme, implicit scheme and boundary-modified scheme are consistent with the analytical solution. The central-difference scheme is less accurate than the previous three methods. The one-sided scheme is only accurate to first order and therefore introduces more error at the short wavelengths, particularly in the horizontal component. The composed scheme goes out of bounds after the computation has run a few steps.

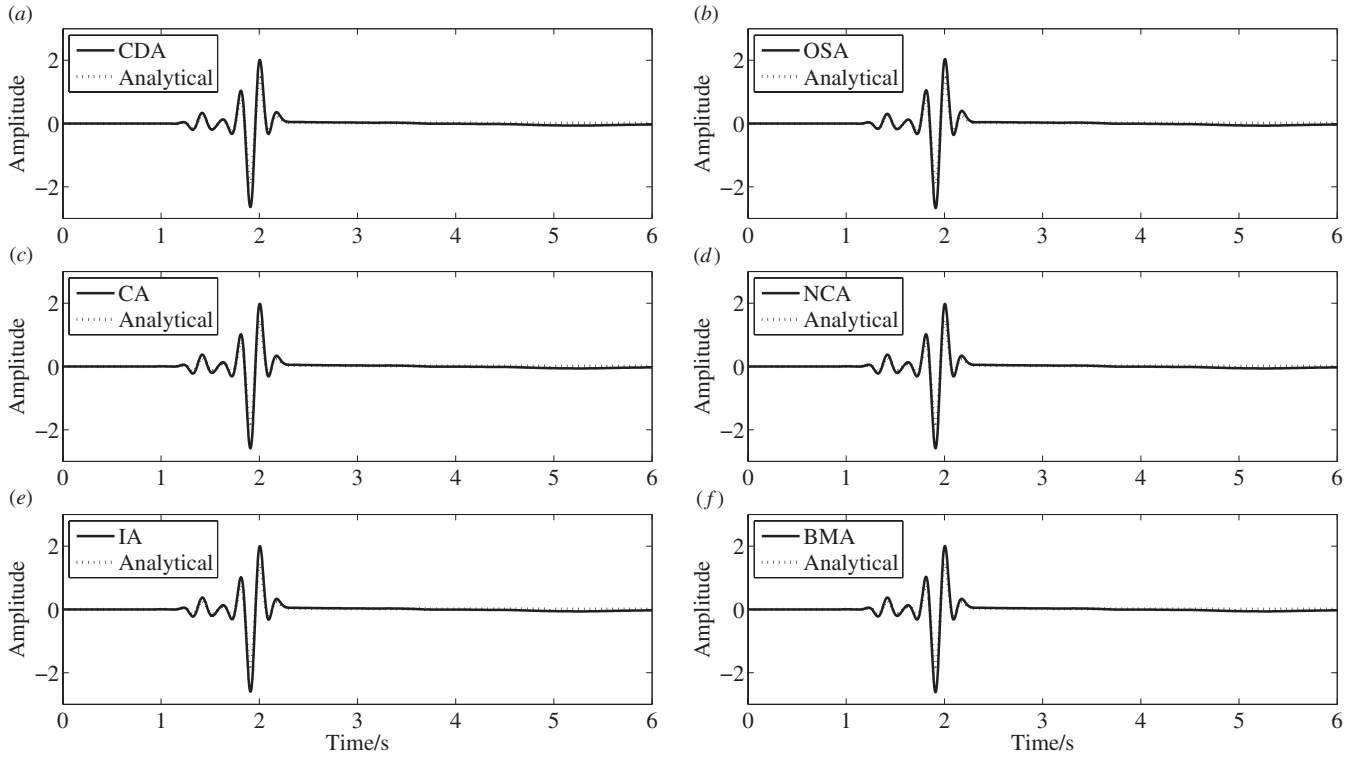

Figure 4. Waveform comparisons of the vertical component between analytical and numerical solutions at the receiver R1 with the source–receiver distance $D = 3$ km for the homogeneous medium model 1. The numerical methods used for comparisons are central-difference, one-sided, composed, new composed, implicit and boundary-modified approximations of the free-surface boundary conditions, respectively.

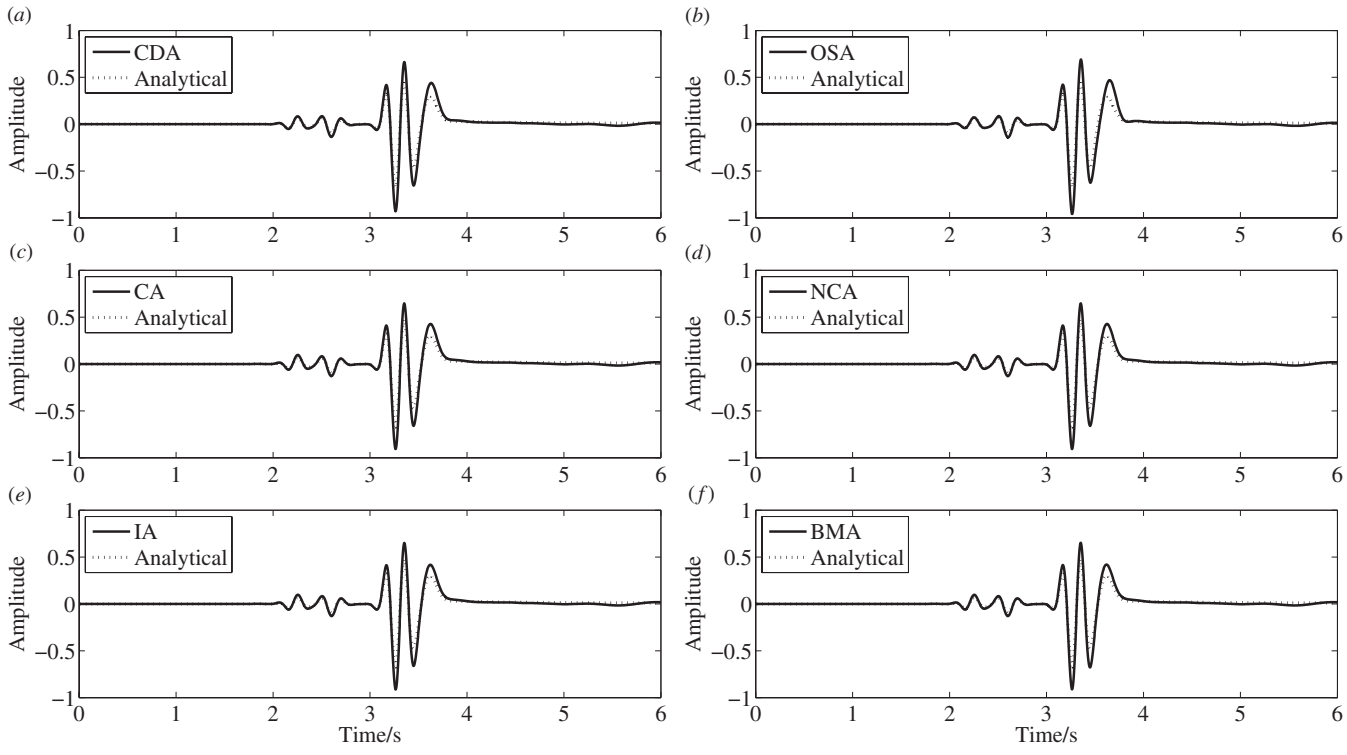

Figure 5. The same as in figure 4 but at the receiver R2 with the source–receiver distance $D = 6$ km.

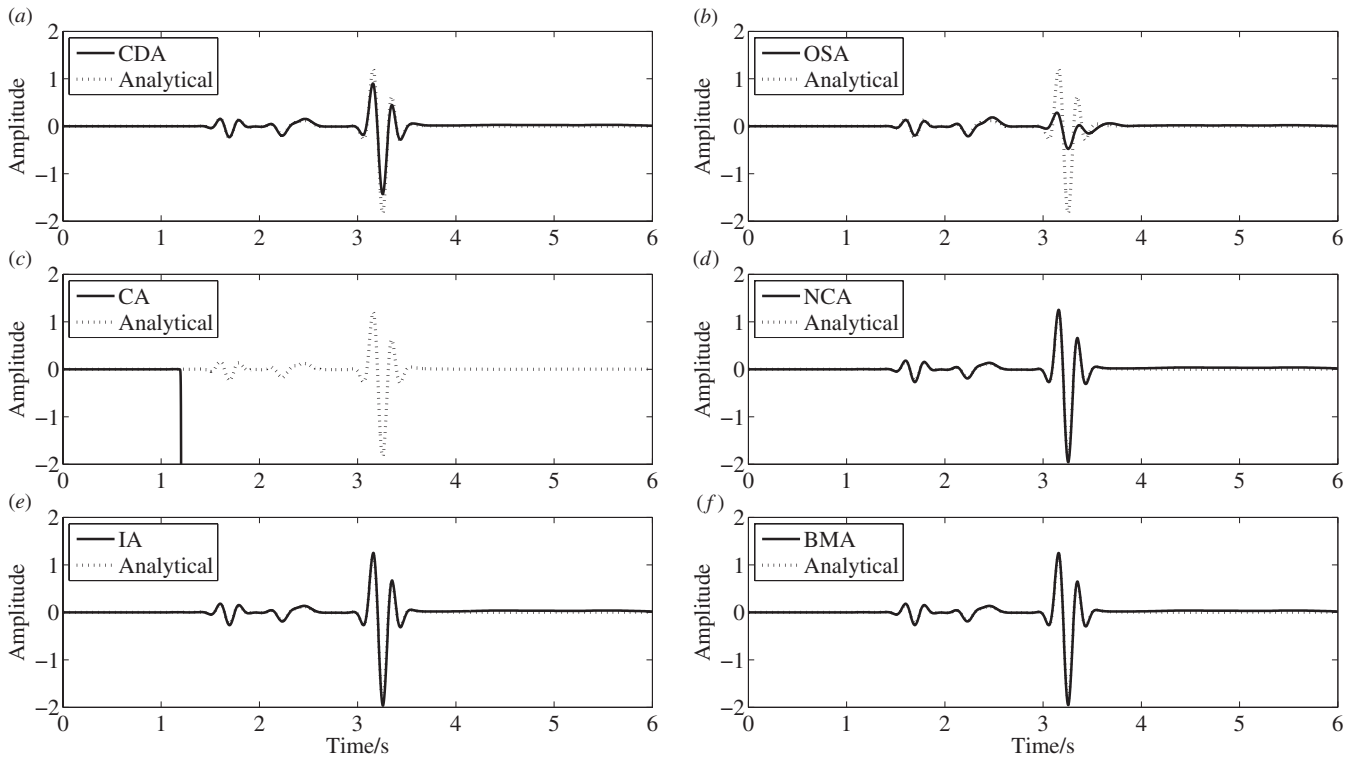

Figure 6. Waveform comparisons of the horizontal component between analytical and numerical solutions at a receiver with the source–receiver distance $D = 4$ km for the homogeneous medium model 2. The numerical methods used for comparison are central-difference, one-sided, composed, new composed, implicit and boundary-modified approximations of the free-surface boundary conditions, respectively.

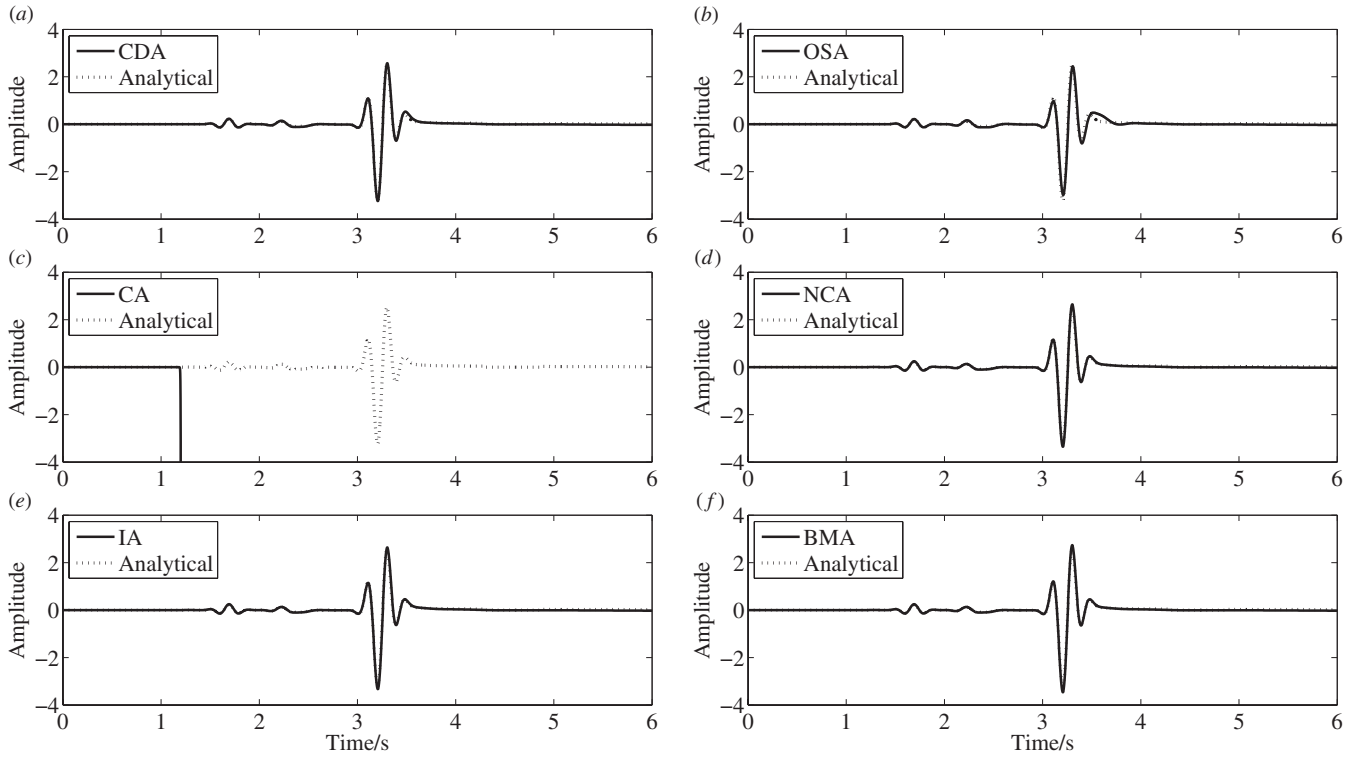

Figure 7. The same as in figure 6 but for the vertical component.

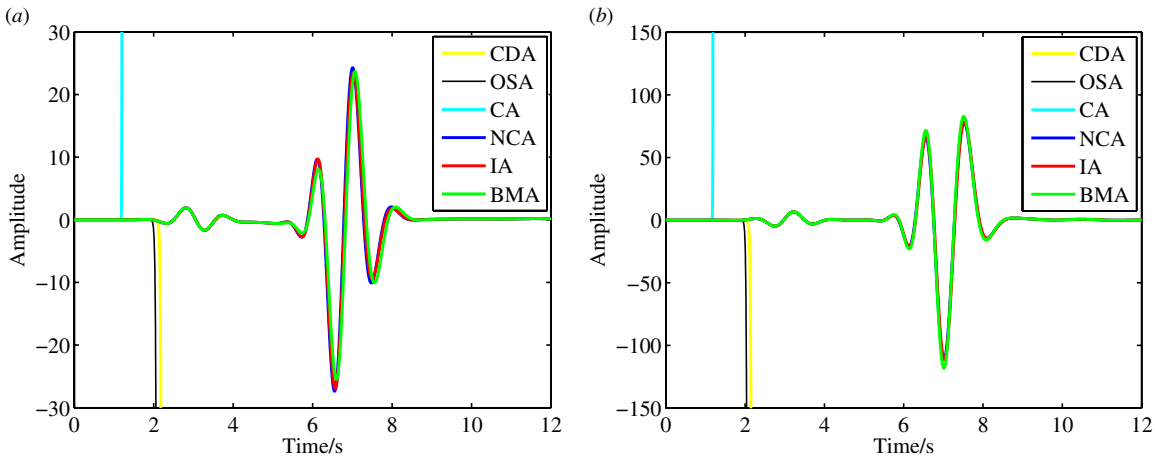

Figure 8. The seismograms recorded at the receiver with the offset of 3 km for the central-difference (CDA), one-sided (OSA), composed (CA), new composed (NCA), implicit (IA) and boundary-modified difference (BMA) approximations of the free-surface boundary conditions are shown for homogeneous medium model 3. (*a*) Horizontal component; (*b*) vertical component.

3.1.3. Model 3. The model with the V_s/V_p of 0.2 has been used to investigate the various free-surface implementations. The P-velocity is 3500 m s^{-1}, the S-velocity 700 m s^{-1}, and the density 1000 kg m^{-3}. The high cut-off frequency is 2 Hz, the time step is 2.5 ms and the grid spacing is 25 m. The receivers with the offset of 3 km are shown in figure 8. The new composed scheme, implicit scheme and boundary-modified scheme also have good agreement. The composed scheme, one-sided scheme and central-difference scheme go out of bounds one after the other. The experiment indicates that the new composed scheme, implicit scheme and boundary-modified scheme are stable and accurate even for the V_s/V_p ratio lower than 0.2.

3.2. A lateral heterogeneous model

A model with lateral heterogeneity is shown in figure 9. In the marked region below the receiver, which is 2.0 km wide and 0.1 km deep, the P-velocity is 1300 m s^{-1}, the S-velocity is 600 m s^{-1}, and the density is 1000 kg m^{-3}. In the rest of the half space, the P-velocity is 3500 m s^{-1}, the S-velocity is 2000 m s^{-1}, and the density is 2600 kgm^{-3}. An explosive source with the high cut-off frequency of 2 Hz is placed at a point located at 1.2 km below and 1 km from the left boundary of the marked region. The time step is 2.5 ms and the grid spacing is 25 m.

The records for the offsets of −2 and 2 km from various implementations of the free-surface boundary condition are shown in figures 10 and 11. Results of the central-difference scheme, one-sided scheme, new composed scheme, implicit scheme and boundary-modified scheme from recorder R1 which is far from the marked region have good agreement. The composed scheme is unstable. The central-difference scheme does not converge after a few minutes of wave propagation. The composed scheme and central-difference scheme go out of bounds earlier in the records located at R2 than those at R1. Reflected waves generated at the top and bottom boundaries of

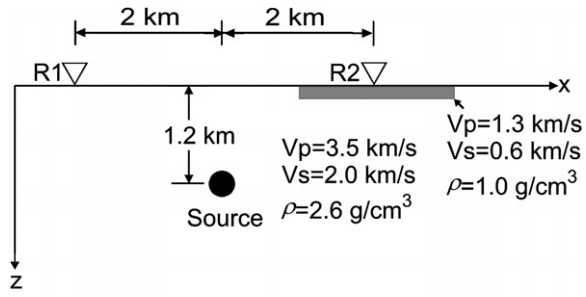

Figure 9. A laterally varying structure.

the marked region. The new composed scheme and boundary-modified scheme have good agreement. Differences between these two explicit schemes and the implicit scheme in the later part of the records arises from the small difference in the free-surface position, which is half a mesh spacing nearer the source in the explicit schemes than in the implicit scheme.

The results have some differences compared with that of Vidale and Clayton (1986), and their results show that the one-sided scheme is not accurate, particularly for the horizontal component. The new composed scheme is slightly unstable. However, in our simulation experiments, the new composed scheme does not appear to be unstable, so their conclusion that the new composed scheme cannot handle laterally varying media properly should be revisited based on our modelling results.

4. Quantitative evaluation of the accuracy of the different free-surface boundary condition approximations

In general, it is better to evaluate the accuracy of the numerical methods in a quantitative way using some reasonably defined error criteria. Here, we use a method proposed by Kristek *et al* (2002) to evaluate the accuracy of the schemes presented

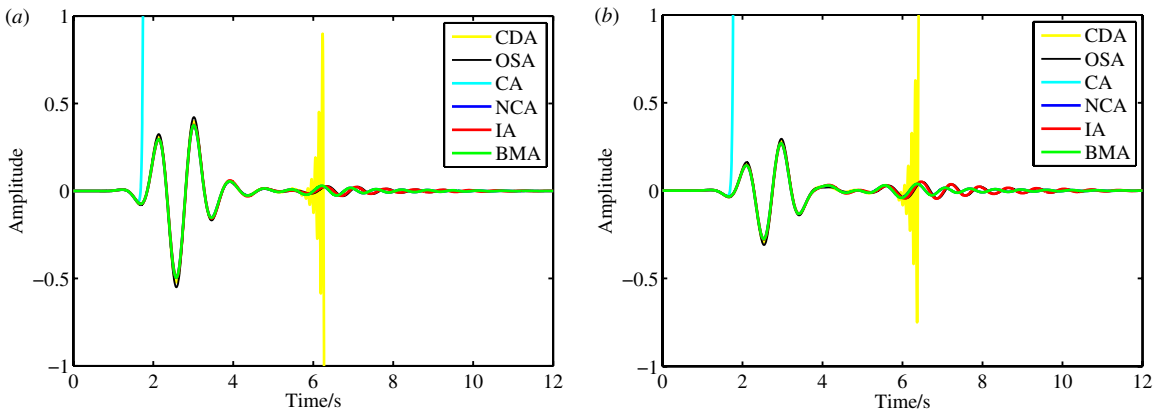

Figure 10. The seismograms recorded at the receiver with the offset of −2 km for the central-difference (CDA), one-sided (OSA), composed (CA), new composed (NCA), implicit (IA) and boundary-modified difference (BMA) approximations of the free-surface boundary conditions are shown for the laterally varying media. (*a*) Horizontal component; (*b*) vertical component.

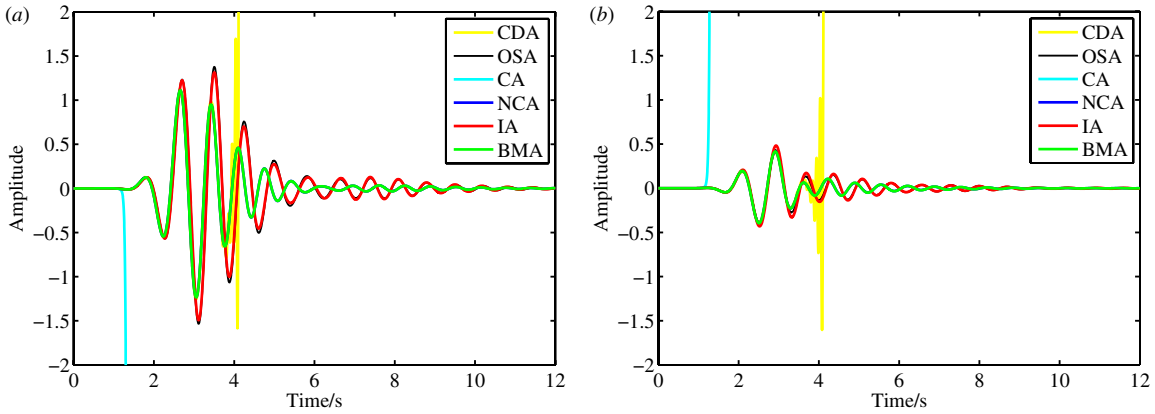

Figure 11. The same as in figure 10 but for the offset of 2 km.

above for simulation of the planar free surface. Let $S(t)$ be the tested solution and $S_{\mathrm{REF}}(t)$ the reference solution.

An integral criterion, say misfit M, can be defined as

$$M = \frac{\sqrt{\sum_m [S_{\mathrm{REF}}(t_m) - S(t_m)]^2}}{\sqrt{\sum_m S^2_{\mathrm{REF}}(t_m)}}. \tag{6}$$

Although the criterion is used for the comparisons of numerical solutions, it is not difficult to check that it accounts more for a phase misfit than for an amplitude misfit. To evaluate the accuracy in both amplitude and phase, Kristek *et al* (2002) defined the envelope misfit EM as

$$\mathrm{EM} = \frac{\sqrt{\sum_m [|\widehat{S}_{\mathrm{REF}}(t_m)| - |\widehat{S}(t_m)|]^2}}{\sqrt{\sum_m |\widehat{S}_{\mathrm{REF}}(t_m)|^2}} \tag{7}$$

and the phase misfit PM as

$$\mathrm{PM} = \frac{\sqrt{\sum_m [|\widehat{S}_{\mathrm{REF}}(t_m)|\mathrm{Arg}(\widehat{S}_{\mathrm{REF}}(t_m) \Big/ \widehat{S}(t_m))]^2}}{\pi \cdot \sqrt{\sum_m |\widehat{S}_{\mathrm{REF}}(t_m)|^2}}, \tag{8}$$

where $\widehat{S}_{\mathrm{REF}}(t)$ and $\widehat{S}(t)$ are analytical signals of $S_{\mathrm{REF}}(t)$ and $S(t)$, respectively, and $\mathrm{Arg}(\varphi)$ is the principal value of the argument of a complex quantity φ.

Figures 12 and 13 show the envelope and phase misfits for the previous figures for all tested methods for the homogeneous models 1 and 2, respectively. The phase misfit for a given source–receiver distance is largest in the one-sided scheme in both models. The misfit values for the horizontal component of model 1 in the central-difference and implicit schemes fluctuate along with the propagation distance, which are smaller than that in the one-sided scheme. The phase misfit for a given source–receiver distance is smallest in the new composed and boundary-modified schemes; the values are relatively close to each other and both less than 0.05, which may indicate that these two methods can give accurate travel-time of a seismic wave field. This is in agreement with the conclusion based on simple visual comparisons of the seismograms.

The envelope misfit is largest in the one-sided solution and smallest in the new composed scheme and boundary-modified solutions. The misfits of the vertical component are smaller than those of the horizontal component, and this may be due to

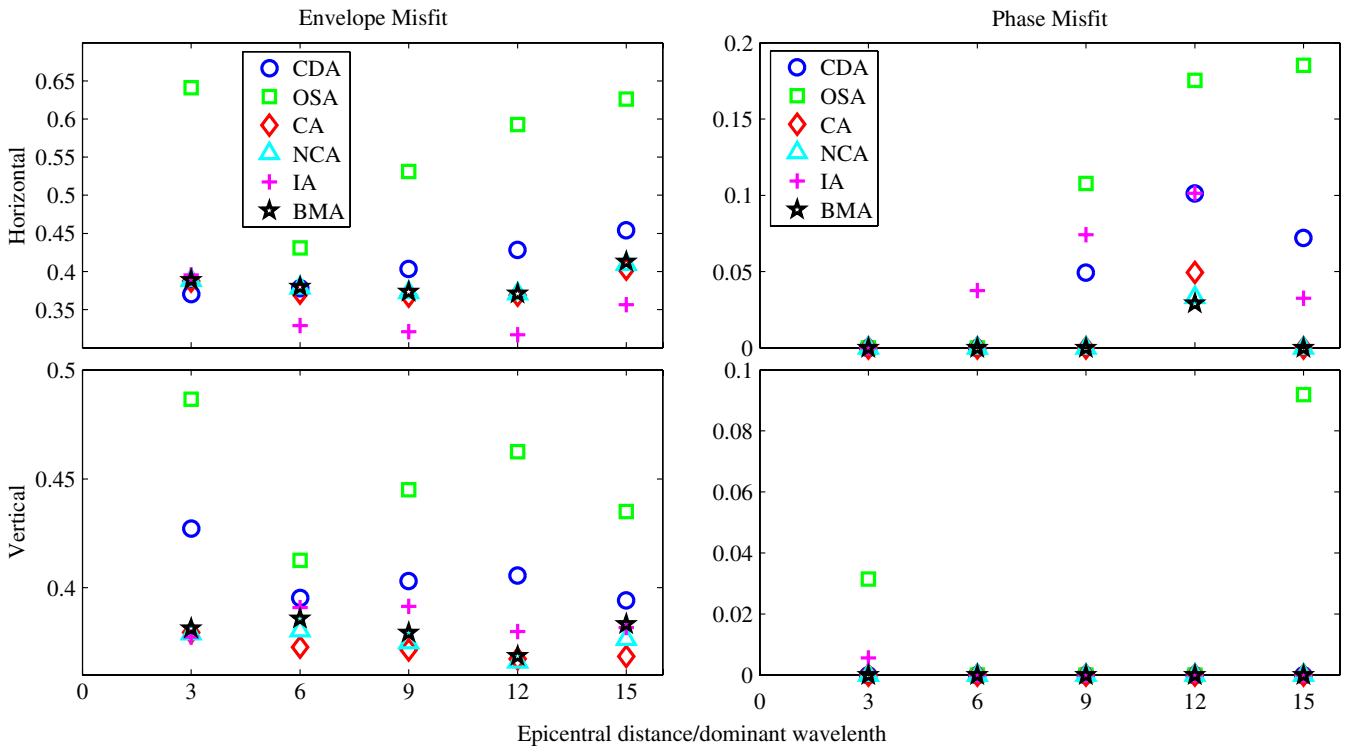

Figure 12. Accuracy of the investigated methods for simulation of the planar free surface of the homogeneous model 1. The envelope and phase misfits are evaluated against the normalized epicentral distance.

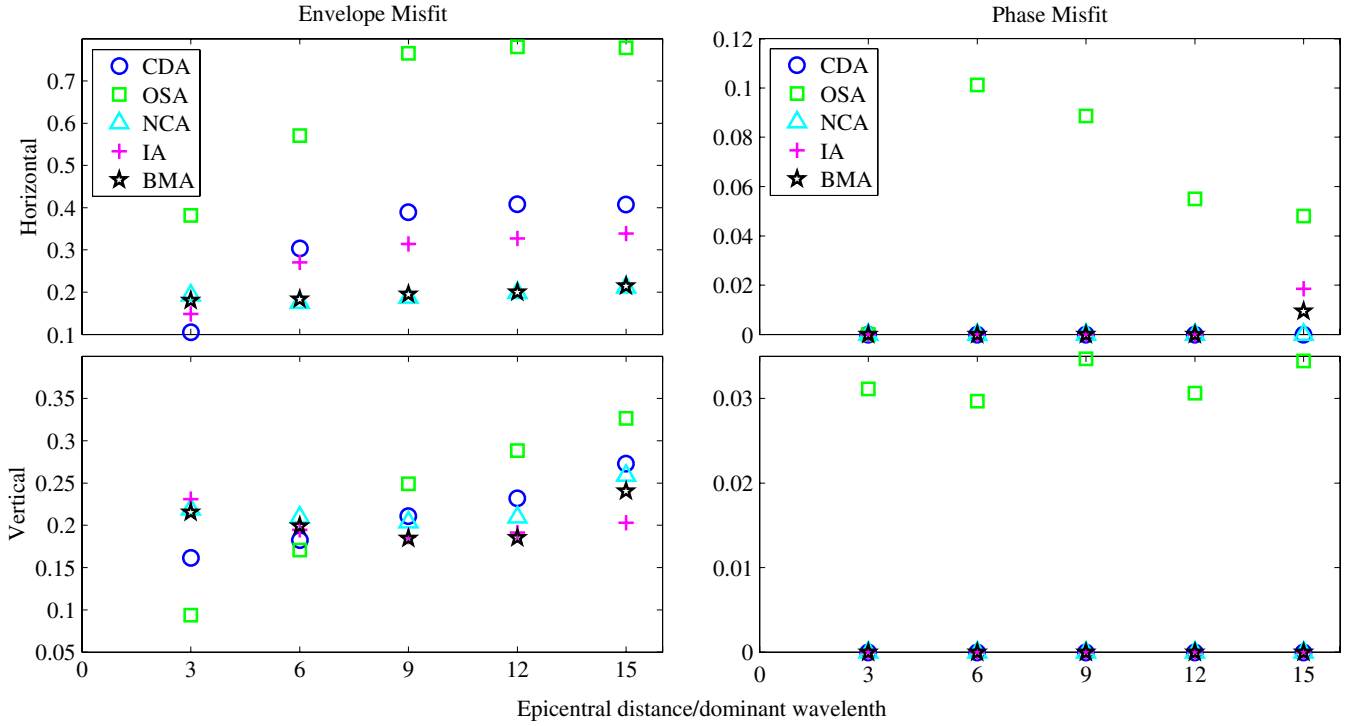

Figure 13. The same as in figure 12 but for the homogeneous model 2.

the source used in the modelling. Considering the differences in phase misfits and envelope misfits of the investigated methods we recommend that the boundary-modified method is slightly better than other methods for simulation of the planar free surface of homogeneous half space.

5. Conclusions

Various free-surface implementations based on the second-order wave equations have been compared. We extend the composed approximation and new composed approximation to

inhomogeneous media. Many of these implementations have been proved to be unstable or to produce inaccurate results. The one-sided scheme is only accurate to the first order and therefore introduces severe error for shorter wavelengths. The central difference and composed scheme are unstable, while the boundary-modified and implicit schemes are stable and accurate for low β/α ratios. Our study here suggests that a stable and explicit approximation scheme to model free surface in seismic modelling in a homogeneous model proposed by Nilsson *et al* (2007) can be extended to inhomogeneous media, and even an irregular free surface.

Acknowledgments

We would like to thank Tao Xu, Kai Liang, Yangfan Deng, Fei Li and Yihe Xu for fruitful discussions. We are especially grateful to Dr Enru Liu for his constructive comments. Three anonymous referees provided valuable comments that helped us improve the manuscript. The Chinese Academy of Sciences (KZCX2-YW-132), the National Natural Science Foundation of China (40721003, 40830315, 40874041 and 41074033), the Important National Science & Technology Specific Projects (2008ZX05008-006) and the Ministry of Science and Technology of China (SINOPROBE-02-02) supported this research.

Appendix A. The central difference, one-sided and implicit approximate schemes

Let $z = 0$ be the free surface of the half space. In the central difference, one-sided and implicit approximations a fictitious line is added parallel to the free surface at $z = -h$. The displacements on the free surface are computed as inner points and the values on the fictitious line are computed from the boundary conditions. It is convenient to denote the squared ratio of the spatial to time increments as $\xi = \frac{\Delta t^2}{h^2}$, and γ as $\frac{\lambda}{\lambda+2\mu}$.

(1) *Centred approximation*:

$$u^p_{i,0} = u^p_{i,2} + \left(v^P_{i+1,1} - v^P_{i-1,1}\right), \tag{A.1}$$

$$v^P_{i,0} = v^P_{i,2} + \gamma\left(u^p_{i+1,1} - u^P_{i-1,1}\right). \tag{A.2}$$

(2) *One-sided approximation*:

$$u^p_{i,0} = u^p_{i,1} + 0.5\left(v^P_{i+1,1} - v^P_{i-1,1}\right), \tag{A.3}$$

$$v^P_{i,0} = v^P_{i,1} + 0.5\gamma\left(u^p_{i+1,1} - u^P_{i-1,1}\right). \tag{A.4}$$

(3) *Implicit approximation*: Applying centred differences to equations (3) and (4), we obtain

$$u^p_{i,0} - \tfrac{1}{4}\left(v^P_{i+1,0} - v^P_{i-1,0}\right) = u^p_{i,1} + \tfrac{1}{4}\left(v^P_{i+1,1} - v^P_{i-1,1}\right), \tag{A.5}$$

$$v^p_{i,0} - \frac{\gamma}{4}\left(u^P_{i+1,0} - u^P_{i-1,0}\right) = v^p_{i,1} + \frac{\gamma}{4}\left(u^P_{i+1,1} - u^P_{i-1,1}\right). \tag{A.6}$$

Equations (A.5) and (A.6) can be further reduced to separate systems for the unknown vectors u_0 and v_0:

$$-\frac{\gamma}{16}u^p_{i+2,0} + \left(1+\frac{\gamma}{8}\right)u^p_{i,0} - \frac{\gamma}{16}u^p_{i-2,0} = \frac{\gamma}{16}u^p_{i+2,1} + \left(1-\frac{\gamma}{8}\right)u^p_{i,1} + \frac{\gamma}{16}u^p_{i-2,1} + \frac{1}{2}(v_{i+1,1} - v_{i-1,1}), \tag{A.7}$$

$$-\frac{\gamma}{16}v^p_{i+2,0} + \left(1+\frac{\gamma}{8}\right)v^p_{i,0} - \frac{\gamma}{16}v^p_{i-2,0} = \frac{\gamma}{16}v^p_{i+2,1} + \left(1-\frac{\gamma}{8}\right)v^p_{i,1} + \frac{\gamma}{16}v^p_{i-2,1} + \frac{\gamma}{2}(u_{i+1,1} - u_{i-1,1}). \tag{A.8}$$

The matrices on the left-hand side of equations (A.7) and (A.8) are pentadiagonal and can be solved rapidly using an algorithm that is a simple extension of the standard tridiagonal solver (Claerbout 1976). The vectors on the right-hand side can be computed from displacements on row 1.

The boundary conditions derived above must be modified for the two extreme edge elements on each side of the free surface, shown as open circles in figure 1(*b*). At these two points, the Bl absorbing boundary conditions of Clayton and Engquist (1977) are applied. For the component u on the left side of the grid, the boundary conditions in equation (A.7) are modified to be

$$(1+\delta)u^p_{0,0} + (1-\delta)u^p_{1,0} = (1-\delta)u^{p-1}_{0,0} + (1+\delta)u^{p-1}_{1,0}, \tag{A.9}$$

$$(1+\delta)u^p_{1,0} + (1-\delta)u^p_{2,0} = (1-\delta)u^{p-1}_{1,0} + (1+\delta)u^{p-1}_{2,0}, \tag{A.10}$$

where $\delta = \alpha\Delta t/h$, Δt is the time step. Here $(u_{0,0}, u_{1,0}, u_{2,0})$ are the first three elements of the vector u_0, and superscripts t and $t-1$ refer to the present and previous time steps. These equations are most effective to absorb horizontally travelling P-waves. Similar equations are used for the vertical component v, except that $\delta = (\beta\Delta t)/h$ is used to absorb horizontally travelling S-waves. The mirror images of these conditions are used at the right edge of the free surface. Equations (A.9) and (A.10) to solve $u_{0,0}$, $u_{1,0}$ are given below

$$u^p_{0,0} = \frac{(1-\delta)^2}{(1+\delta)^2}u^p_{2,0} + \frac{(1-\delta)}{(1+\delta)}u^{p-1}_{0,0} + u^{p-1}_{1,0} - \frac{(1-\delta)^2}{(1+\delta)^2}u^{p-1}_{1,0} - \frac{(1-\delta)}{(1+\delta)}u^{p-1}_{2,0}, \tag{A.11}$$

$$u^p_{1,0} = -\frac{1-\delta}{1+\delta}u^p_{2,0} + \frac{1-\delta}{1+\delta}u^{p-1}_{1,0} + u^{p-1}_{2,0}. \tag{A.12}$$

Appendix B. The composed approximate scheme

In this paper, we extend this method to heterogeneous media.

Differentiating equations (3) and (4) with respect to x, we obtain

$$u_{xz} = -v_{xx}, \tag{B.1}$$

$$v_{xz} = -\frac{\lambda}{\lambda+2\mu}u_{xx}. \tag{B.2}$$

Substituting equations (B.1) and (B.2) in the wave equations (1) and (2), we can obtain

$$\rho\frac{\partial^2 u}{\partial t^2}=\frac{\partial}{\partial x}\left((\lambda+2\mu)\frac{\partial u}{\partial x}\right)-\frac{\lambda}{\lambda+2\mu}\frac{\partial\lambda}{\partial x}\frac{\partial u}{\partial x}+\mu\frac{\partial^2 u}{\partial z^2}-\frac{\lambda(\lambda+\mu)}{\lambda+2\mu}\frac{\partial^2 u}{\partial x^2}, \tag{B.3}$$

$$\rho\frac{\partial^2 v}{\partial t^2}=\frac{\partial}{\partial x}\left(\mu\frac{\partial v}{\partial x}\right)-\frac{\partial\mu}{\partial x}\frac{\partial v}{\partial x}-(\lambda+\mu)\frac{\partial^2 v}{\partial x^2}-\frac{\lambda}{\lambda+2\mu}\frac{\partial(\lambda+2\mu)}{\partial z}\frac{\partial u}{\partial x}+(\lambda+2\mu)\frac{\partial^2 v}{\partial z^2}+\frac{\partial\lambda}{\partial z}\frac{\partial u}{\partial x}. \tag{B.4}$$

The displacements are expanded around a surface point $(i, 1)$ into the following Taylor series:

$$u(i,2,p)=u(i,1,p)+hu_z(i,1,p)+\tfrac{1}{2}h^2u_{zz}(i,1,p)+O(h^3), \tag{B.5}$$

$$v(i,2,p)=v(i,1,p)+hv_z(i,1,p)+\tfrac{1}{2}h^2v_{zz}(i,1,p)+O(h^3). \tag{B.6}$$

Using the boundary conditions (3) and (4), wave equations (B.3) and (B.4) to replace the first and second derivatives respectively, and then using the central differences to approximate the x derivatives, we finally obtain the explicit finite difference equations for the displacements on the free surface:

$$\begin{aligned}u_{i,1}^{p+1}=&\,2[1-\frac{\mu_{i,1}}{\rho_{i,1}}\xi+\frac{\lambda_{i,1}(\lambda_{i,1}+\mu_{i,1})}{\rho_{i,1}(\lambda_{i,1}+2\mu_{i,1})}\xi]u_{i,1}^{p}-u_{i,1}^{p-1}\\&+2\xi\frac{\mu_{i,1}}{\rho_{i,1}}u_{i,2}^{p}+\frac{1}{2\rho_{i,1}}\xi\{[(\lambda_{i,1}+2\mu_{i,1})\\&+(\lambda_{i+1,1}+2\mu_{i+1,1})](u_{i+1,1}^{p}-u_{i,1}^{p})-[(\lambda_{i,1}+2\mu_{i,1})\\&+(\lambda_{i-1,1}+2\mu_{i-1,1})](u_{i,1}^{p}-u_{i-1,1}^{p})\}\\&-\frac{1}{4}\frac{\lambda_{i,1}}{\rho_{i,1}(\lambda_{i,1}+2\mu_{i,1})}\xi(\lambda_{i+1,1}-\lambda_{i-1,1})(u_{i+1,1}^{p}-u_{i-1,1}^{p})\\&-\frac{\lambda_{i,1}(\lambda_{i,1}+\mu_{i,1})}{\rho_{i,1}(\lambda_{i,1}+2\mu_{i,1})}\xi(u_{i+1,1}^{p}+u_{i-1,1}^{p})\\&+\xi\frac{\mu_{i,1}}{\rho_{i,1}}(v_{i+1,1}^{p}-v_{i-1,1}^{p}),\end{aligned} \tag{B.7}$$

$$\begin{aligned}v_{i,1}^{p+1}=&\,2\left(1-\frac{\mu_{i,1}}{\rho_{i,1}}\xi\right)v_{i,1}^{p}-v_{i,1}^{p-1}+2\xi\frac{\lambda_{i,1}+2\mu_{i,1}}{\rho_{i,1}}v_{i,2}^{p}\\&-\frac{(\lambda_{i,1}+\mu_{i,1})}{\rho_{i,1}}\xi(v_{i+1,1}^{p}+v_{i-1,1}^{p})+\xi\frac{\lambda_{i,1}}{\rho_{i,1}}(u_{i+1,1}^{p}-u_{i-1,1}^{p})\\&+\frac{1}{2\rho_{i,N}}\xi[(\mu_{i,1}+\mu_{i+1,1})(v_{i+1,1}^{p}-v_{i,1}^{p})\\&-(\mu_{i,1}+\mu_{i-1,1})(v_{i,1}^{p}-v_{i-1,1}^{p})]\\&-\frac{1}{4\rho_{i,1}}\xi(\mu_{i+1,1}-\mu_{i-1,1})(v_{i+1,1}^{p}-v_{i-1,1}^{p})\\&-\frac{1}{2\rho_{i,1}}\xi\frac{\lambda_{i,1}}{\lambda_{i,1}+2\mu_{i,1}}[(\lambda_{i,2}+2\mu_{i,2})\\&-(\lambda_{i,1}+2\mu_{i,1})](u_{i+1,1}^{p}-u_{i-1,1}^{p})\\&+\frac{\xi}{2}(\lambda_{i,2}-\lambda_{i,1})(u_{i+1,1}^{p}-u_{i-1,1}^{p}).\end{aligned} \tag{B.8}$$

For homogeneous media the equations can be reduced to

$$\begin{aligned}u_{i,1}^{p+1}=&\,2\left[1-2\xi\beta^2\left(2-\frac{\beta^2}{\alpha^2}\right)\right]u_{i,1}^{p}-u_{i,1}^{p-1}+2\xi\beta^2u_{i,2}^{p}\\&+\xi\beta^2\left(3-\frac{2\beta^2}{\alpha^2}\right)(u_{i+1,1}^{p}+u_{i-1,1}^{p})+\xi\beta^2(v_{i+1,1}^{p}-v_{i-1,1}^{p}),\end{aligned} \tag{B.9}$$

$$\begin{aligned}v_{i,1}^{p+1}=&\,2(1-2\xi\beta^2)v_{i,1}^{p}-v_{i,1}^{p-1}+2\xi\alpha^2v_{i,2}^{p}\\&-\xi\alpha^2\left(1-\frac{2\beta^2}{\alpha^2}\right)(v_{i+1,1}^{p}+v_{i-1,1}^{p})\\&+\xi\alpha^2\left(1-\frac{2\beta^2}{\alpha^2}\right)(u_{i+1,1}^{p}-u_{i-1,1}^{p}).\end{aligned} \tag{B.10}$$

Numerical modelling results indicate that the method is unstable when the ratio of the S- to P-wave velocities (V_s/V_p) is less than 0.57 (Ilan *et al* 1975). Ilan and Loewenthal (1976) supported that the formula for v on the surface is responsible for the instability of the composed method. They also proposed a revised method and the vertical component of the displacement has been changed in the following manner.

Appendix C. The new composed approximate scheme

The vertical component of the displacement is expanded around a surface point $(i, 1)$ into the following Taylor series:

$$v(i,2,p)=v(i,1,p)+h\frac{\partial v(i,1,p)}{\partial z}+\frac{1}{2}h^2\frac{\partial^2 v(i,1,p)}{\partial z^2}+O(h^3). \tag{C.1}$$

The boundary condition (3) and the equation of motion (2) are rewritten in the forms

$$\frac{\partial v}{\partial z}=\frac{\lambda}{\lambda+2\mu}\frac{\partial u}{\partial x}, \tag{C.2}$$

$$\frac{\partial^2 v}{\partial z^2}=\frac{1}{\lambda+2\mu}\left(\rho\frac{\partial^2 v}{\partial t^2}-\frac{\partial}{\partial x}\left(\mu\frac{\partial v}{\partial x}\right)+\frac{\partial\mu}{\partial x}\frac{\partial v}{\partial x}-(\lambda+\mu)\frac{\partial^2 u}{\partial x\partial z}-\frac{\partial(\lambda+2\mu)}{\partial z}\frac{\partial v}{\partial z}-\frac{\partial\lambda}{\partial z}\frac{\partial u}{\partial x}\right). \tag{C.3}$$

Substituting equations (C.2) and (C.3) into equation (C.1) gives a new formula, and then replacing x and t derivatives by central finite differences and z derivative by the forward difference we obtain an explicit equation for v on the free surface:

$$\begin{aligned}v_{i,1}^{p+1}=&-v_{i,1}^{p-1}+2\left[1-\frac{\lambda_{i,1}+2\mu_{i,1}}{\rho_{i,1}}\xi\right]v_{i,1}^{p}+2\frac{\lambda_{i,1}+2\mu_{i,1}}{\rho_{i,1}}\xi v_{i,2}^{p}\\&+\frac{\xi}{\rho_{i,N}}\lambda_{i,1}(u_{i+1,1}^{p}-u_{i-1,1}^{p})\\&+\frac{\xi}{2\rho_{i,1}}[(\mu_{i,1}+\mu_{i+1,1})(v_{i+1,1}^{p}-v_{i,1}^{p})\\&+(\mu_{i,1}+\mu_{i-1,1})(v_{i-1,1}^{p}-v_{i,1}^{p})]\\&+\frac{\xi}{2\rho_{i,1}}[\mu_{i+1,1}(u_{i+1,2}^{p}-u_{i+1,1}^{p})+\mu_{i-1,1}(u_{i-1,1}^{p}-u_{i-1,2}^{p})]\end{aligned}$$

$$+\frac{\xi}{2\rho_{i,1}}\left[\lambda_{i,2}\left(u^p_{i+1,2}-u^p_{i-1,2}\right)+\lambda_{i,1}\left(u^p_{i-1,1}-u^p_{i+1,1}\right)\right]$$
$$-\frac{\xi}{2\rho_{i,1}}\frac{\lambda_{i,1}}{\lambda_{i,1}+2\mu_{i,1}}\left[\left((\lambda_{i,2}+2\mu_{i,2})\right.\right.$$
$$\left.\left.-(\lambda_{i,1}+2\mu_{i,1})\right)\left(u^p_{i+1,1}-u^p_{i-1,1}\right)\right]. \quad \text{(C.4)}$$

For homogeneous media the equation is reduced to

$$v^{p+1}_{i,1}=-v^{p-1}_{i,1}+2[1-\xi(\beta^2+\alpha^2)]v^p_{i,1}+2\xi\alpha^2v^p_{i,2}$$
$$+\xi\beta^2\left(v^p_{i+1,1}+v^p_{i-1,1}\right)+0.5\xi(\alpha^2-3\beta^2)\left(u^p_{i+1,1}-u^p_{i-1,1}\right)$$
$$+0.5\xi(\alpha^2-\beta^2)\left(u^p_{i+1,2}-u^p_{i-1,2}\right). \quad \text{(C.5)}$$

Appendix D. The boundary-modified approximate scheme

In this scheme, a one-sided operator is used on the boundary for the approximation of the normal derivative in $\partial_x\partial_z$ and $\partial_z\partial_x$ cross derivatives (in 2D as an example), and displacement components at the free-surface boundary are approximated as the following expressions:

$$u^{p+1}_{i,1}=2u^p_{i,1}-u^{p-1}_{i,1}+\frac{\xi}{2}\left[\left(\alpha^2_{i+1,1}+\alpha^2_{i,1}\right)\left(u^p_{i+1,1}-u^p_{i,1}\right)\right.$$
$$\left.-\left(\alpha^2_{i,1}+\alpha^2_{i-1,1}\right)\left(u^p_{i,1}-u^p_{i-1,1}\right)\right]$$
$$+\frac{\xi}{2}\left[\left(\beta^2_{i,2}+\beta^2_{i,1}\right)\left(u^p_{i,2}-u^p_{i,1}\right)-\left(\beta^2_{i,1}+\beta^2_{i,0}\right)\left(u^p_{i,1}-u^p_{i,0}\right)\right]$$
$$+\frac{\xi}{2}\left[\alpha^2_{i+1,1}\left(v^p_{i+1,2}-v^p_{i+1,1}\right)-\alpha^2_{i-1,1}\left(v^p_{i-1,2}-v^p_{i-1,1}\right)\right]$$
$$-\xi\left[\beta^2_{i+1,1}\left(v^p_{i+1,2}-v^p_{i+1,1}\right)-\beta^2_{i-1,1}\left(v^p_{i-1,2}-v^p_{i-1,1}\right)\right]$$
$$+\frac{\xi}{2}\left[\beta^2_{i,2}\left(v^p_{i+1,2}-v^p_{i-1,2}\right)-\beta^2_{i,1}\left(v^p_{i+1,1}-v^p_{i-1,1}\right)\right], \quad \text{(D.1)}$$

$$v^{p+1}_{i,1}=2v^p_{i,1}-v^{p-1}_{i,1}+\frac{\xi}{2}\left[\left(\beta^2_{i+1,1}+\beta^2_{i,1}\right)\left(v^p_{i+1,1}-v^p_{i,1}\right)\right.$$
$$\left.-\left(\beta^2_{i,1}+\beta^2_{i-1,1}\right)\left(v^p_{i,1}-v^p_{i-1,1}\right)\right]$$
$$+\frac{\xi}{2}\left[\left(\alpha^2_{i,2}+\alpha^2_{i,1}\right)\left(v^p_{i,2}-v^p_{i,1}\right)-\left(\alpha^2_{i,1}+\alpha^2_{i,0}\right)\left(v^p_{i,1}-v^p_{i,0}\right)\right]$$
$$+\frac{\xi}{2}\left[\alpha^2_{i,2}\left(u^p_{i+1,2}-u^p_{i-1,2}\right)-\alpha^2_{i,1}\left(u^p_{i+1,1}-u^p_{i-1,1}\right)\right]$$
$$-\xi\left[\beta^2_{i,2}\left(u^p_{i+1,2}-u^p_{i-1,2}\right)-\beta^2_{i,1}\left(u^p_{i+1,1}-u^p_{i-1,1}\right)\right]$$
$$+\frac{\xi}{2}\left[\beta^2_{i+1,1}\left(u^p_{i+1,2}-u^p_{i+1,1}\right)-\beta^2_{i-1,1}\left(u^p_{i-1,2}-u^p_{i-1,1}\right)\right]. \quad \text{(D.2)}$$

The free-surface boundary conditions can be discretized as

$$\tfrac{1}{2}[(\mu)_{i,3/2}D^z_+u_{i,1}+(\mu)_{i,1/2}D^z_+u_{i,0}]+(\mu)_{i,1}D^x_0v_{i,1}=0, \quad \text{(D.3)}$$

$$\tfrac{1}{2}[(\lambda+2\mu)_{i,3/2}D^z_+v_{i,1}+(\lambda+2\mu)_{i,1/2}D^z_+v_{i,0}]$$
$$+(\lambda)_{i,1}D^x_0u_{i,1}=0, \quad \text{(D.4)}$$

$i=1,\ldots,N_x$.

At first glance, it may appear that using a one-sided operator the accuracy of the method would be reduced to the first order. However, as it was theoretically shown in Nilsson *et al* (2007), a first-order error on the boundary in the differential equations (D.1) and (D.2) can be absorbed as a second-order perturbation of the boundary conditions (D.3) and (D.4).

References

Alterman Z S and Karal F 1968 Propagation of elastic waves in layered media by finite difference methods *Bull. Seismol. Soc. Am.* **58** 367–98

Alterman Z S and Rotenberg A 1969 Seismic waves in a quarter plane *Bull. Seismol. Soc. Am.* **59** 347–68

Berenger J 1994 A perfectly matched layer for the absorption of electromagnetic waves *J. comput. phys.* **114** 185–200

Cao S and Greenhalgh S 1998 Attenuating boundary conditions for numerical modeling of acoustic wave propagation *Geophysics* **63** 231–43

Cerjan C, Kosloff D, Kosloff R and Resef M 1985 A nonreflecting boundary condition for discrete acoustic and elastic wave equations *Geophysics* **50** 705–8

Chen J and Bording R P 2010 Application of the nearly perfectly matched layer to the propagation of low-frequency acoustic waves *J. Geophys. Eng.* **7** 277–83

Claerbout J 1976 *Fundamentals of Geophysical Data Processing* (New York: McGraw-Hill)

Clayton R W and Enquist B 1977 Absorbing boundary conditions for acoustic and elastic wave equations *Bull. Seismol. Soc. Am.* **67** 1529–40

Crank J and Nicolson P 1996 A practical method for numerical evaluation of solutions of partial differential equations of the heat-conduction type *Adv. Comput. Math.* **6** 207–26

De Hoop A 1960 A modification of Cagniard's method for solving seismic pulse problems *Appl. Sci. Res.* B **8** 349–56

Engquist B and Majda A 1977 Absorbing boundary conditions for the numerical simulation of waves *Math. Comput.* **31** 629–51

Higdon R L 1991 Absorbing boundary conditions for elastic waves *Geophysics* **56** 231–41

Ilan A 1978 Stability of finite difference schemes for the problem of elastic wave propagation in a quarter plane *J. Comput. Phys.* **29** 389–403

Ilan A and Loewenthal D 1976 Instability of finite difference schemes due to boundary conditions in elastic MEDIA* *Geophys. Prospect.* **24** 431–53

Ilan A, Ungar A and Alterman Z S 1975 An improved representation of boundary conditions in finite difference schemes for seismological problems *Geophys. J. R. Astron. Soc.* **43** 727–45

Kelly K, Ward R, Treitel S and Alford R 1976 Synthetic seismograms: a finite-difference approach *Geophysics* **41** 2–7

Komatitsch D and Tromp J 2003 A perfectly matched layer absorbing boundary condition for the second-order seismic wave equation *Geophys. J. Int.* **154** 146–53

Kristek J, Moczo P and Archuleta R 2002 Efficient methods to simulate planar free surface in the 3D 4th-order staggered-grid finite-difference schemes *Stud. Geophys. Geod.* **46** 355–81

Lamb H 1904 On the propagation of tremors over the surface of an elastic solid *Phil. Trans. R. Soc. (London)* A **203** 1–42

Lan H Q and Zhang Z J 2011 Three-dimensional wave-field simulation in heterogeneous transversely isotropic medium with irregular free surface *Bull. Seismol. Soc. Am.* at press

Liao Z P, Wong H L, Yang B P and Yuan Y F 1984 A transmitting boundary for transient wave analysis *Sci. Sin.* A **27** 1063–76

Nilsson S, Petersson N, Sj green B and Kreiss H 2007 Stable difference approximations for the elastic wave equation in second order formulation *SIAM J. Numer. Anal.* **45** 1902–36

Reynolds A C 1978 Boundary conditions for the numerical solution of wave propagation problems *Geophysics* **43** 1099–110

Tian X B, Kang I, Kim G and Zhang H 2008 An improvement in the absorbing boundary technique for numerical simulation of elastic wave propagation *J. Geophys. Eng.* **5** 203–9

Vidale J and Clayton R 1986 A stable free-surface boundary condition for two-dimensional elastic finite-difference wave simulation *Geophysics* **51** 2247–9

Wu G and Liang K 2005 Combined boundary conditions of quasi-P wave within frequency-space domain in VTI media *Geophys. Prospect. Pet.* **44** 301–7 (in Chinese)

Yang D H, Liu E, Zhang Z and Teng J 2002 Finite-difference modelling in two-dimensional anisotropic media using a flux-corrected transport technique *Geophys. J. Int.* **148** 320–8

Yang D H, Wang S, Zhang Z and Teng J 2003 n-Times absorbing boundary conditions for compact finite-difference modeling of acoustic and elastic wave propagation in the 2D TI medium *Bull. Seismol. Soc. Am.* **93** 2389–401

Zhang Z J, He Q and Xu Z 1993 Absorbing boundary condition for FD modeling in 2D inhomogeneous TIM *Chin. J. Geophys.* **36** 519–27

Zhang Z J, Wang G and Harris J 1999 Multi-component wavefield simulation in viscous extensively dilatancy anisotropic media *Phys. Earth Planet. Inter.* **114** 25–38